Numerical and experimental studies of turbulent particle-laden gas flow in an in-line tube bank

J. Y. Tu,* C. A. J. Fletcher,[†] Y. S. Morsi,[‡] W. Yang[‡] and M. Behnia[§]

*Australian Nuclear Science and Technology Organisation (ANSTO), Lucas Heights Science and Technology Centre, NSW 2234, Australia;
[†]Centre for Advanced Numerical Computation in Engineering and Science (CANCES),
The University of New South Wales, Sydney 2052, Australia;
[‡]School of Mechanical and Manufacturing Engineering, Swinburne University of Technology,
PO Box 218 Hawthorn, Victoria 3122 Australia;
[§]School of Mechanical and Manufacturing Engineering, The University of New South Wales,
Sydney 2052, Australia

Abstract—Turbulent particle-laden gas flow in an in-line tube bank is studied, computationally and experimentally. An Eulerian model with generalised Eulerian boundary conditions for the particulate phase is employed. In the momentum balance equations, the particulate phase momentum exchanges with solid walls are included. The turbulent effects of the gas phase are taken into account using a renormalization group (RNG) based k–ε turbulence model while the particulate turbulent diffusivity is related to the turbulent viscosity of the gas phase. The experiment is performed in an in-line tube bank located in a horizontal wind tunnel, using laser-Doppler Anemometry (LDA). The comparison of numerical predictions with experimental data is made for the mean axial and transverse velocity profiles of both phases, the turbulent intensity of the gas phase, and the distribution of particle concentration in the tube bank. Very good agreement with experimental data is obtained for computed values of the mean velocity of both gas and particulate phases, and the particulate concentration distribution. Interesting information is also presented which shows the different flow behaviour demonstrated by the gas and particulate phases, in particular for larger particles. © 1997 Elsevier Science Ltd

Keywords: RNG k–ε turbulence model; turbulent particle-laden gas flow; in-line tube bank; tube bundle erosion.

1. INTRODUCTION

Current interest in design, operation and maintenance of energy conversion systems has focussed attention on turbulent particle-laden gas flows. Reducing erosion and enhancing heat transfer in the design of tube banks and heat exchangers to be located in fluidised beds and advanced coal-fired combustors is crucial for their successful development. It is important to investigate the hydrodynamics of fluid and particle motion for a better understanding of tube bundle erosion, and the influence of the presence of solid particles on the fluid flow which may affect the heat transfer performance.

Considerable computational research has been undertaken for the cases of a single tube (e.g. Celik et al., 1985) and tube banks (e.g. Faghri and Rao, 1987) in single-phase flow. The investigation of a two-phase flow around a cylinder under the simplifying assumption such as viscous or inviscid gas flow was carried out (Morsi and Alexander, 1972; Ilias and Douglas, 1989). Vittal and Tabakoff (1987) studied the same problem at low Reynolds number, while Laitone (1981) developed a vortex method and analysed the flow of gas and particles around a cylinder at high Reynolds numbers. More recently, the flow of a dilute particle-laden gas moving past one or two in-line tubes undergoing erosion has been studied numerically by Schuh et al. (1989) and Fan et al. (1991). However, there is no numerical study of turbulent particle-laden gas flow in tube banks which makes a direct comparison with experimental data.

In this paper, both numerical and experimental studies are reported for turbulent gas–particle flow in an in-line tube bank. An Eulerian model, with generalized Eulerian boundary conditions for the particulate phase (Tu and Fletcher, 1995a, b), is employed for the numerical calculations of the gas–particle flows in a tube bank. The experimental work is carried out by the use of laser-Doppler Anemometry

(LDA) in an in-line tube bank located in a horizontal wind tunnel. In order to model experimentally the fluid flow and particulate behaviour, the mean and fluctuating velocity profiles of both gas and particulate phases, and the particle concentration distribution are measured, with glass spheres of 66 and 93 μm in diameter employed to represent the particulate phase.

Computational prediction of the turbulent gas-particle flow in a tube bank presents a very difficult problem. Mostly, the trajectory model (Lagrangian approach) has been used for computation of the particulate phase (e.g. Schuh *et al.*, 1989; Fan *et al.*, 1991). Although the Lagrangian approach is a more fundamental procedure to describe the particle–wall collision process and can yield a detailed physical description of the individual particles such as particle speeds and trajectories, the particle paths which result from a Lagrangian description often do not contain enough information for engineers. From an engineering design perspective, the mean particulate flow fields need to be known in terms of mean particulate velocities and the distribution of particle concentration, to facilitate quantifiable decisions. Therefore, the continuum model (Eulerian approach) becomes attractive as an alternative way of representing the particulate phase to obtain the mean particulate flow fields. In addition, the effects of interactions between the two phases (two-way coupling) are more easily considered by using the Eulerian approach (e.g. Chen and Wood, 1985; Tu and Fletcher, 1994).

One of the difficulties encountered in using the Eulerian formulation for the particulate phase in complex flow domains is modelling the boundary conditions at solid surfaces. This has been resolved (Tu and Fletcher, 1995a) by establishing a set of Eulerian-formulation, generalised wall boundary conditions and by developing a particle–wall collision model to represent particle–wall momentum transfers. Then the complex two-phase flow, where the mean particulate flow behaviour near the surface of a wall depends significantly on the interaction of particles with the wall, can be simulated appropriately. The effects of gas-phase turbulence are taken into account by using a renormalization group (RNG) based k–ε turbulence model (Orszag *et al.*, 1993). The particulate turbulent diffusivities are modelled by using the gradient hypothesis relating to the gas-phase turbulence (Chen and Wood, 1985; Adeniji-Fashola and Chen, 1990). Thus, the flow in both the gas and particulate phases is represented by a generic formulation (Fletcher, 1993) which can be solved efficiently using a high-order finite volume discretisation (Cho and Fletcher, 1991).

It is worthwhile noting that this type of formulation of the governing equations for the particulate phase is used in a number of engineering calculations (e.g. Melvlle and Bray, 1979; Pourahmadi and Humphrey, 1983; Rizk *et al.*, 1993). Recent analysis by Reeks (1993) and simulation by Simonin *et al.* (1994) for a model Couette flow problem suggests that the turbulence modelling may be simplified if Favre (mass-weighted) averaging is used instead of Reynolds

averaging and that the use of an isotropic eddy viscosity for the particulate phase may not be appropriate for certain classes of low-loading flow at intermediate Stokes number. Although turbulence modelling for gas–particle two-phase flows is very important, it is expected that particle–wall interactions will be a primary controlling factor for the current wall-dominated gas–particle flow with a relative high Stokes number.

The contribution of the present paper is that a two-fluid model (Chen and Wood, 1985; Adeniji-Fashola and Chen, 1990) is employed in combination with the developed particle–wall collision model and the Eulerian boundary conditions for the particulate phase (Tu and Fletcher, 1995b, Tu *et al.*, 1997). The measurements provide the mean and fluctuating velocities of both gas and particulate phases, and particle concentration distribution in an in-line tube bank. The numerical predictions are compared with the LDA measurements. The experimental data for two different particle sizes are presented to illustrate their different flow behaviour from the gas flow through the tube bank.

The following section describes the theoretical model, including the equations solved, RNG based k–ε turbulence model applied, particle–wall momentum transfer implemented, boundary conditions specified, and the solution algorithm used. In the section describing the experimental study, the flow configuration and the instrumentation used to obtain the measurements are indicated. The uncertainity of experimental measurements for both the gas and particulate phases are discussed. Then, the comparisons of the computed results with LDA measurements are given. Finally, the particulate flow behaviour in terms of the mean and fluctuating velocity profiles in the tube bank are discussed.

2. MATHEMATICAL MODEL

2.1. *Governing equations*

In an Eulerian model, both gas and particulate phases are considered as continua and a set of Reynolds-averaged conservation equations for the mass and momentum of both phases, gas kinetic energy of turbulence and its dissipation rate can be written in a generic transport form (Tu and Fletcher, 1995a):

$$\frac{\partial}{\partial x_j}(A_i \phi) - \frac{\partial}{\partial x_j}\left(B \frac{\partial \phi}{\partial x_j}\right) = S. \qquad (1)$$

Gas phase: Continuity equation ($\phi = 1$)

$$A_i = \rho_g u_g^i; \qquad B = 0; \qquad S = 0 \qquad (2)$$

Momentum equation ($\phi = u_g^i$)

$$A_i = \rho_g u_g^i; \qquad B = \rho_g \nu_{g,\text{eff}}; \qquad S = -\frac{\partial P}{\partial x_i} - F_D. \qquad (3)$$

Turbulent kinetic energy equation ($\phi = k$)

$$A_i = \rho_g u_g^i; \qquad B = \alpha \rho_g \nu_{gt}; \qquad S = P_k - \rho_g \varepsilon + S_k. \qquad (4)$$

ε-equation ($\phi = \varepsilon$)

$$A_i = \rho_g u_g^i; \qquad B = \alpha \rho_g v_{gt};$$

$$S = \frac{\varepsilon}{k}(C_{\varepsilon 1} P_k - C_{\varepsilon 2} \rho_g \varepsilon) - R + S_\varepsilon. \qquad (5)$$

Particulate phase: Continuity equation ($\phi = \rho_p$)

$$A_i = \rho_p u_p^i; \qquad B = \rho_p D_p;$$

$$S = \left[\rho_p u_p^i - D_p \frac{\partial \rho_p}{\partial x_i} \right] \frac{\partial \rho_p}{\partial x_i}. \qquad (6)$$

Momentum equation ($\phi = u_p^i$)

$$A_i = \rho_p u_p^i; \qquad B = \rho_p v_p;$$

$$S = \frac{\partial}{\partial x_i}\left(\rho_p v_p \frac{\partial u_p^j}{\partial x_i} \right) + \frac{\partial}{\partial x_j}\left[D_p \left(u_p^j \frac{\partial \rho_p}{\partial x_i} + u_p^i \frac{\partial \rho_p}{\partial x_j} \right) \right]$$

$$+ F_D + F_G + F_{WM}. \qquad (7)$$

In the above governing equations, it is assumed that since the particulate phase is dilute, interparticle collision is negligible. The second-order turbulence correlation terms due to the averaging process have been modelled using a gradient hypothesis (Chen and Wood, 1985)

$$- \overline{\rho_p' u_p^{i'}} = D_p \frac{\partial \rho_p}{\partial x_i}$$

$$- \rho_p \overline{u_p^{i'} u_p^{j'}} = \mu_p \left(\frac{\partial u_p^i}{\partial x_j} + \frac{\partial u_p^j}{\partial x_i} \right) \qquad (8)$$

where the particulate turbulent diffusivities D_p and μ_p are related to the turbulent viscosity of the gas phase v_{gt} by (Adeniji-Fashola and Chen, 1990)

$$D_p = \frac{v_p}{S_c}; \qquad v_p = \frac{\mu_p}{\rho_p} = K_p v_{gt} \qquad (9)$$

and S_c is the turbulent Schmidt number taken to be 0.7. K_p is a weight factor accounting for the particle inertia which is given by

$$K_p = \max[K_d, 1/(1 + S_t^i)] \qquad (10)$$

where K_d is a numerical dissipation and S_t^i is the turbulent Stokes number, $= t_p/t_e$. Here t_p is a particle response or relaxation time given by $t_p = \rho_s d_p^2/18\rho_g v_l$, where ρ_s is the material density of particles, d_p the diameter of the particle and v_l laminar viscosity of gas phase. The eddy characteristic time follows the work of Adeniji-Fashola and Chen (1990) for the confined two-phase flow, $t_e = 0.125 \, k/\varepsilon$. Thus, K_p is reflecting the transfer of turbulent energy to the particulate phase due to the particle inertia. In some regions, particularly near the wall, this value becomes very small (less than 0.001) so that K_d is taken to be 0.01 to avoid numerical instability because the particulate flow with less than 1% turbulent diffusivity of the gas turbulent viscosity is already convection dominated. The choice of the different coefficients in the formula for the time scale of turbulence t_e, such as used in

Chen and Wood (1985) or Adeniji-Fashola and Chen (1990) is insensitive for the case of experimental comparison.

A recently developed turbulence model, the dynamic renormalization group theory (RNG) based k–ε turbulence model (Orszag et al., 1993) is employed in this study. The RNG-based k–ε turbulence model because of the nature of the derivation, is expected to be applicable to a wide range of flow situations. In the RNG turbulent transport equation, an inverse Prandtl number α is introduced, and the rate of strain term R in the ε-equation is expressed as

$$R = \frac{C_\mu \eta^3 (1 - \eta/\eta_0)}{1 + \beta \eta^3} \frac{\varepsilon^2}{k} \quad \text{and} \quad \eta = \frac{k}{\varepsilon}(2S_{ij}^2)^{1/2},$$

$$S_{ij} = \frac{1}{2}\left(\frac{\partial u_g^i}{\partial x_j} + \frac{\partial u_g^j}{\partial x_i} \right) \qquad (11)$$

where $\beta = 0.015$, $\eta_0 = 4.38$. According to the RNG theory (Yakhot and Orzag, 1986), the constants in the turbulent transport equations are given to be $\alpha = 1.39$, $C_\mu = 0.0845$, $C_{\varepsilon 1} = 1.42$ and $C_{\varepsilon 2} = 1.68$, respectively.

The effects of particles on the gas turbulence are taken into account through the following source terms (Tu and Fletcher, 1994):

$$S_k = -2k(\rho_p/t_p)[1 - \exp(-B_k t_p/t_L)] \qquad (12)$$

in the k equation and

$$S_\varepsilon = -2\varepsilon(\rho_p/t_p)[1 - \exp(-B_\varepsilon t_p/t_e)] \qquad (13)$$

in the ε equation, where $B_k = 0.09$, $B_\varepsilon = 0.4$ and $t_L = k/\varepsilon$.

For a dilute suspension, the viscous and pressure terms in the particulate phase momentum equations are neglected. But a particle–wall momentum exchange in terms of a momentum source term F_{WM} is included to model the particle–wall interactions. The momentum exchange source term is given (Tu and Fletcher, 1995a) by

$$F_{WM}^N = -C_N[1 + (e_p^{-N})^2] \rho_p |W_{p,h}^N| W_{p,h}^N (B^N)^2 A_n \qquad (14)$$

in the normal direction and

$$F_{WM}^T = -C_T[1 - (e_p^{-T})^2] \rho_p |W_{p,h}^T| W_{p,h}^T (B^T)^2 A_n$$

$$\qquad (15)$$

in the tangential direction. Here, A_n denotes a face area of the control volume coincident with the wall. e_p^{-N} annd e_p^{-T} are normal and tangential mean restitution coefficients, respectively. $W_{p,h}^N$ and $W_{p,h}^T$ are normal and tangential mean velocities of particulate phase at the distance h away from the wall. B^N and B^T are constants related to the restitution coefficients (Tu and Fletcher, 1995a). C_N and C_T are coefficients which are modelled by

$$C_N = C_m \frac{W_{p,h}^N}{[\sum_{i=1}^3 (u_{p,h}^i)^2]^{1/2}} \qquad (16)$$

where C_m is referred to as the particle inertial impacting efficiency which is similar to that obtained by Ilias

and Douglas (1989) based on the particle inertia (Stokes number, S_t) and the Reynolds number of the gas phase. Referring to the work of Ilias and Douglas, for the present case $C_m = 0.9$ is chosen.

The coefficient C_T is related to the tangential wall-momentum exchange which is modelled as

$$C_T = \frac{C_N}{y^+} \quad \text{for } y^+ \leqslant 11.63$$
$$C_T = \frac{C_N \kappa}{\ln(Ey^+)} \quad \text{for } y^+ > 11.63 \tag{17}$$

where κ and E are the same as in the turbulence model of gas phase (Launder and Spalding, 1974), 0.41 and 9.0, respectively, and y^+ has a similar definition, but for the particulate flow (Soo, 1984). Alternatively, the tangential coefficient C_T can be modelled by relating it to the wall friction (Sommerfeld, 1992). The effect of both the normal and tangential wall-momentum exchanges on the particulate flow is only included for control volumes immediately adjacent to the wall.

The gravity force is $F_G = \rho_p g$, where g is the gravitational acceleration. The drag force F_D is defined by

$$F_D^i = \rho_p \frac{f(u_g^i - u_p^i)}{t_p} \tag{18}$$

where t_p is the particle relaxation time and the correction factor f is selected according to Schuh et al. (1989) as

$$f = \begin{cases} 1 + 0.15 Re_p^{0.687}, & 0 < Re \leqslant 200 \\ 0.914 Re_p^{0.282} + 0.0135 Re_p, & 200 < Re_p \leqslant 2500 \\ 0.0167 Re_p, & 2500 < Re_p \end{cases} \tag{19}$$

with the particulate Reynolds number defined by

$$Re_p = \frac{|u_g^i - u_p^i| d_p}{v_g}. \tag{20}$$

2.2. Boundary conditions

The boundary conditions at the inlet are specified for all dependent variables in both the gas and particulate phases. At outflow and symmetry planes the normal gradient of these quantities is set to zero. A 'no-slip' boundary condition is employed for the gas velocity at the wall surface. The boundary conditions at the solid wall for the particulate phase are based on the generalised wall boundary equations which can be written in a generic form (Tu and Fletcher, 1995a) as

$$a\varphi_w + b\left[\frac{\partial \varphi}{\partial n}\right]_w = c, \qquad \varphi = [W_p^N, W_p^T, \rho_p] \tag{21}$$

where n indicates the direction normal to the surface of the wall. The coefficients in the equation can be determined as follows

$$a_N = A^N - B^N; \qquad b_N = A^N Kn_h; \qquad c_N = 0$$
$$a_T = A^T - B^T; \qquad b_T = A^T Kn_h; \qquad c_T = 0 \tag{22}$$
$$a_\rho = B^N - A^N; \qquad b_\rho = A^N Kn_h; \qquad c_\rho = 0$$

where

$$A^N = \left[\frac{1.0 + e_p^{-N}(-e_p^{-N})^q}{2}\right]^{1/(q+1)};$$

$$A^T = \left[\frac{1.0 + (e_p^{-T})^{q+1}}{2}\right]^{1/(q+1)}$$

$$B^N = \left\{\frac{e_p^{-N}[1.0 + (-e_p^{-N})^q]}{1.0 + e_p^{-N}}\right\}^{1/(q+1)};$$

$$B^T = \left\{\frac{e_p^{-N} + (e_p^{-T})^{q+1}}{1.0 + e_p^{-N}}\right\}^{1/((q+1)}$$

$$(23)$$

where $q = 2$ corresponds to an energy average. Kn_h is a Knudsen number defined by a gas-particle interaction length divided by the system characteristic length, $Kn_h = h(l_{gp}/L_D)$. For turbulent flow following (Soo, 1984), $l_{gp} = t_p|W_R'|$, where $|W_R'|$ is the modulus of the relative turbulence intensity between the gas and particulate phase. In the present work, we take the slip velocity $|W_R|$ instead of the relative turbulence because it is found from our experimental observations that this approximation is reasonable for the particulate flow near tube surface.

2.3. Numerical procedure

Equation (1) is discretised using a finite volume formulation in generalised coordinate space with the metric information expressed in terms of area vectors. The equations are solved on a non-staggered grid. The velocity components in fixed Cartesian directions are treated as scalars after the transformation from physical coordinates to computational space coordinates. To approximate the convective terms at faces of the control volumes, a generalised QUICK convective differencing method (Cho et al., 1991) is used. Second derivatives are evaluated using three-point symmetric formulae. Each governing equation is sequentially relaxed to update one of the primitive variables. A velocity potential correction (Fletcher and Bain, 1991) is introduced to satisfy continuity of gas phase and upgrade the gas pressure using a modified SIMPLE algorithm (Van Doormaal and Raithby, 1984). The stored values at the centroids are interpolated and modified to calculate the flow flux at faces of the control volumes using the moment interpolation method (Rhie and Chow, 1983). The governing equations for both the gas and particulate phase are solved sequentially at each iteration to obtain all the dependent variables. At each global iteration each equation is iterated, using a Strongly Implicit Procedure (Fletcher, 1991).

3. EXPERIMENTAL STUDY

There is very little work reported in the literature on the use of LDA to determine flow and particle characteristics in an in-line tube bank. There are, however, a number of investigations related to the staggered tube arrangement (Nowshiravani et al., 1982; Simoneau and VanFossen, 1984). Recently

comprehensive experimental work for the cross flow development in a staggered tube bank under high Reynolds number conditions was reported by Halim and Turner (1986). Using LDA the mean velocity components and turbulence parameters were measured for the developing regions along the tube bank. However, measurements were only taken at centre-lines in each of the tube rows. Morsi et al. (1995) have reported a fully detailed experimental program of measuring the flow fields through an in-line tube bank model. They have given the time mean and turbulent parameter measurements for different Reynolds numbers together with particle size distributions. Here only a brief description and a selected sample of data will be given.

3.1. The test facility

A schematic of the experimental facility used in this study is shown in Fig. 1. Briefly, it consists of a model of an in-line tube bank mounted inside a rectangular cross section of an open circuit wind tunnel. The transparent walls of the working section have a cross-section area of 360 mm × 500 mm. Air is drawn into the test section by means of centrifugal fan through a honeycomb bellmouth entry. A filter system was incorporated in the tunnel exhaust to facilitate the removal of the particles.

As shown in Fig. 2, the tube bank model consists of a 6 × 6 array of carbon steel tube of 25 mm OD, and was constructed to simulate the arrangement of a regular bank of boiler tubes. The horizontal distance between tube centres, i.e. the longitudinal pitch P_l is 75 mm, and the vertical distance between tube centers, i.e. the transverse pitch is 50 mm. Thus the ratio between the longitudinal pitch and the tube diameter is 3, and the ratio between the transverse pitch and the tube diameter is 2.

At the beginning of each experiment the bank model was aligned in the direction of the main stream of the flow and the velocity was set, with the aid of
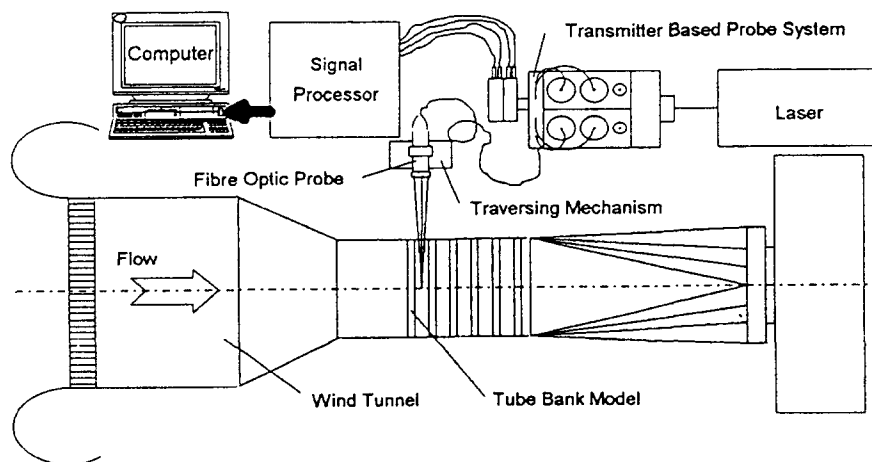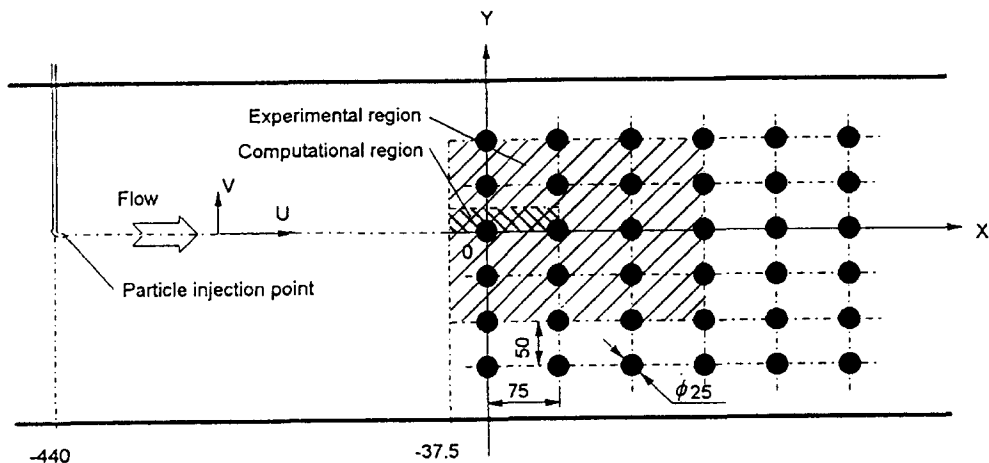

Fig. 1. Schematic of the experimental setup.

Fig. 2. The tube bank test section.

a speed controller, to $U_b = 11.2$ m/s. The turbulence intensity of the main stream was about 2.2%. The velocity of the gas phase was measured separately from particulate velocity.

3.2. Laser doppler anemometry

A schematic representation of the Dantec two-component LDA system is shown in Fig. 1. This system consists of a two color four beam optical arrangement utilizing the green (wave length = 514.5 nm) and blue (wave length = 488 nm) lines of a 5 W Argon-Ion laser. The fibre optic had a lens of a 400 mm focal length and a 38 mm beam separation which produced an ellipsoid shaped measurement volume with diameter of 0.194 mm and a length of 4.09 mm, while the 40 MHz frequency shift introduced to one of the crossing beams from each color facilitated measuring flow reversals in the wake regions of the tube bank. This system is capable to determine simultaneously the time mean axial and transverse velocities U and V, as well as the RMS of the fluctuating components, $\sqrt{\overline{u^2}}$ and $\sqrt{\overline{v^2}}$, of the flow.

All the measurements were taken in x-z plan where the fibre optic probe was traversed parallel to the tube bank by a three-dimensional traversing mechanism in the main region of the flow. To avoid the tube blockage near tube wall region, the probe was angled toward the wall by 2.7° as shown in Fig. 3. This enabled taking measurements up to 4 mm from the tube surface.

The traversing measurements were taken vertically each 5 mm along the Y-axis beginning from 37.5 mm upstream of the first tube row and traversing 7.5 mm each line along the X-axis until the center of the fourth tube row downstream. Figure 2 shows the experimental measurement region for gas and particulate phase and the computational region for comparison with measurements.

3.3. Particle seeding apparatus

Since the source of signals in LDA system is the scattering particle, geometric and physical parameters of the particles influence the quality of signals

obtained from the photodetector of the system. For instance if the particles are small enough ($St \ll 1.0$) the particles are in dynamic equilibrium with the flow so that the particle velocity essentially equals the local gas velocity. For larger particles that are not in dynamic equilibrium, there is a slip velocity that is a function of the particle size, relative density, geometry and velocity. Therefore, in choosing the correct seeding one must ensure that the particles are small enough to follow the flow an yet large enough to generate sufficient scattered light of good quality for signal processing.

As discussed by Menon and Lai (1991), another important physical parameter which must be considered, in optimising the quality of the signal, is the relative refractive index of a particle that is the ratio of the refractive indices of the particle and the medium. Such a ratio describes the ability to scatter light for selecting particles.

For the gas phase, the air was seeded with glycol smoke tracer particles. The glycol smoke was generated by a smoke generator and then injected into the wind tunnel from its inlet. The low density particles (of 0.5 μm in mean diameter) tracked the gas flow well within the limit of accuracy of the measurement. Their high refractive index was useful in maximizing the signal-to-noise ratio (SNR) and hence obtaining the maximum data rate and most accurate information.

The solid particles used in this study were spherical glass particles ($\rho_s = 2990$ kg/m^3) with particle sizes of 66 and 93 μm. A fluidised feeder was specially designed for this experiment whereby the solid particles were injected into the system in a controllable manner. The internal pressure of fluidising vessel was monitored and maintained at 240 kPa force the particles via a flexible lose hose through a nozzle into the wind tunnel.

The maximum bulk solids/gas mass loading ratio, defined as the mass flow rate of particles divided by the mass flow rate of air, was less than 0.1 kg/kg. In this experimental study, only the core flow region of the jet was used. In this region, the particulate concentration distribution was found to be reasonably uniform.

3.4. LDA experimental techniques

Table 1 lists the general technical data of the LDA fiber optic probe system used for the current study.

All measurements were taken with a Bragg cell in the beam path to introduce a 40 MHz frequency shift to one of the beams. This eliminates the directional ambiguity that would be present in the wake regions of the tubes. Frequencies this high are difficult to measure accurately with the counter-type-processor. The processor of the LDA system used here is known as Burst Spectrum Analyzer (BSA) which has the ability to distinguish the dominant frequency from background noise. For instance, the BSA type of Dantec 58N10 signal processor used in the current study was capable of handling data rate in excess of 170,000 velocity measurements per second, which is
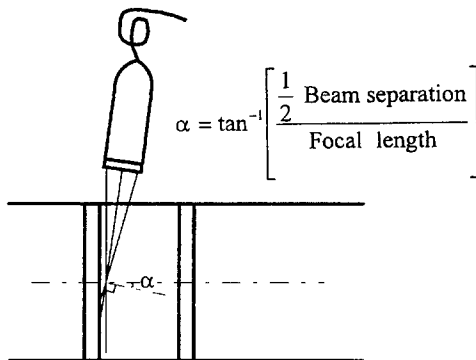

$$\alpha = \tan^{-1}\left[\frac{\frac{1}{2}\text{ Beam separation}}{\text{Focal length}}\right]$$

Fig. 3. Sketch of the inclined probe in near tube wall regions (not to scale).

Table 1. Technical data of the LDA system

	Blue beam	Green beam
Laser wavelength, λ (nm)	488	514.5
Focal length (mm)	400	400
Beam separation (mm)	38	38
Diameter of laser beam waist (mm)	1.35	1.35
Beam intersection angle, θ ($^\circ$)	21.5	21.5
Diameter of focussed laser beam (μm)	46	48.5
Diameter of measuring volume (mm)	0.184	0.1943
Length of measuring volume (mm)	3.88	4.09
Fringe separation, δ_f (μm)	5.143	5.422
Number of fringes	36	36

fast enough to deal with all flow conditions in this study.

All the data points obtained here were based on samples of 2000 and elapsed time of 30 s. The stop mode was set on validated 2000 samples while the dead time mode was turned off to ensure that data acquisition terminated with the number of validated samples to be collected. The presentation and analysis of this data was carried out with the aid of a software package called SIZEware. The method of data processing was the residence times of the individual scattering particles. The axial and transverse time mean velocities, U and V, and the RMS values of axial and transverse fluctuation components, $\sqrt{\overline{u^2}}$ and $\sqrt{\overline{v^2}}$, were calculated using the following equations:

$$U = \frac{\sum_{i=1}^{N} U_i \Delta t_i}{\sum_{i=1}^{N} \Delta t_i} \qquad (24a)$$

$$V = \frac{\sum_{i=1}^{N} V_i \Delta t_i}{\sum_{i=1}^{N} \Delta t_i} \qquad (24b)$$

$$\sqrt{\overline{u^2}} = \left[\frac{\sum_{i=1}^{N} (U_i - U)^2 \Delta t_i}{\sum_{i=1}^{N} \Delta t_i} \right]^{1/2} \qquad (25a)$$

$$\sqrt{\overline{v^2}} = \left[\frac{\sum_{i=1}^{N} (V_i - V)^2 \Delta t_i}{\sum_{i=1}^{N} \Delta t_i} \right]^{1/2} \qquad (25b)$$

in which the subscript i denotes the ith particle, N is the number of particles (so-called sample size) and Δt is the transit time of ith particle for residence time weighting.

3.6. Experimental uncertainty

For the gas phase velocity measurement, the smoke used has 0.5 μm in mean diameter, and an aerodynamic response time of approximately 10 μs. This would respond quite effectively to the smallest time scale fluctuations in the flow. Hence any error from this source is considered to be negligible.

Measuring frequency of the LDA bursts which depends primarily on laser wave length and the cross angle of the beams can introduce some errors. Although the error associated with the wave length for the Argon Ion laser is negligible, the beam crossing angle (which is determined by the beam spacing and the focal length of the lens) can introduce some uncertainty in the real velocity. A beam spacing of 38 mm used in this experimental study is assumed to have an error of $\pm$ 0.5 mm, which can introduce an uncertainty in the real velocity of 1%. However, the error due to uncertainty of the optical configuration is constant and affects all measurements equally.

The errors associated with the two seeding particles in the measurement volume can be considered negligible (Durst et al., 1981). This because the two particles will have very similar Doppler frequencies so the wave length of the beat frequency will be much longer than the time of sampling. Scattering from multiple particles can also cause uncertainty, however, the recent developed processors such as the type of BSA processor used in this investigation ensure that such scattering signals are rejected.

In particle-laden flow, the largest source of error is primarily due to the cross talk where the large particle velocity may be measured as a fluid tracer velocity. For a single point measurement the difference between the local velocity and the particle velocity may be largely due to the unresponsiveness of the heavy particles to small scale motions. However, most experimentalist are aware of this, and many numbers of samples are taken to reduce the uncertainty of the ensemble statistics.

In estimating the uncertainty for the mean velocity, the Student-t distribution (Bendat and Piersol, 1971; Sakakibara et al., 1995) was used. The uncertainty is given by

$$\left(\bar{x} - \frac{st}{\sqrt{N}} \right) \leqslant \mu_x \leqslant \left(\bar{x} + \frac{st}{\sqrt{N}} \right) \qquad (26)$$

where (x is the true mean, $\bar{x}$ the simple mean, N the sample size, s the sample standard deviation and t the area under the Student-t distribution for the given value of N($t = 1.96$ for 95% confidence as $N \rightarrow \infty$).

In this study all LDA measurements used 2000 samples with 95% confidence level the uncertainty of time mean axial and transverse velocities measurements in gas phase was 0.0044 times the measured standard deviation. The uncertainty on the turbulence measurements primarily depends on the number of samples and the confidence interval. The uncertainty may be estimated to be around $\pm 5\%$.

Another well known source of uncertainty is velocity bias which has been examined widely by many researchers. It occurs because the LDA approximates the statistics of the flow by the sample statistics of the measured particle realizations. When the velocity fluctuates, the volume flow rate through the measuring volume varies with the velocity magnitude and direction. Given a spatially uniform distribution of seeding particles, the rate of validated measurements varies in proportion to the volume flow rate through the measuring volume. Arithmetic averaging of the resultant velocity realizations will therefore produce a

velocity result biased to a higher value than the actual flow velocity. The residence time weighting method which is known to reduce the error associated with velocity bias has been adapted here.

In summary all the above errors have been provided and may be stated that the estimated measure-

ment error of the mean velocity is about $\pm 3\%$ and the rms is maximum $\pm 7\%$.

4. RESULTS AND DISCUSSION

The objective of the experimental program is to provide a data base that could be used to validate the
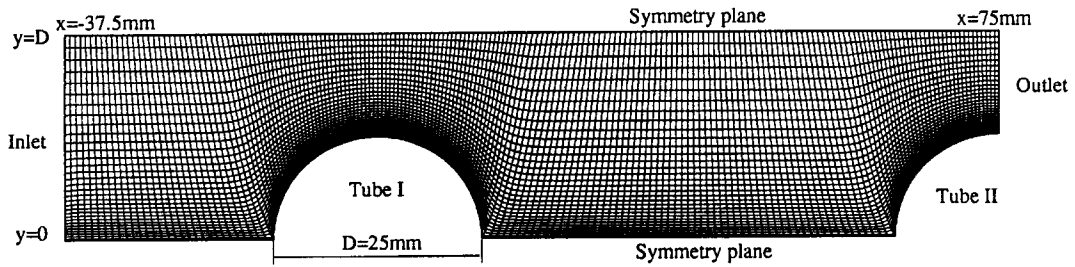

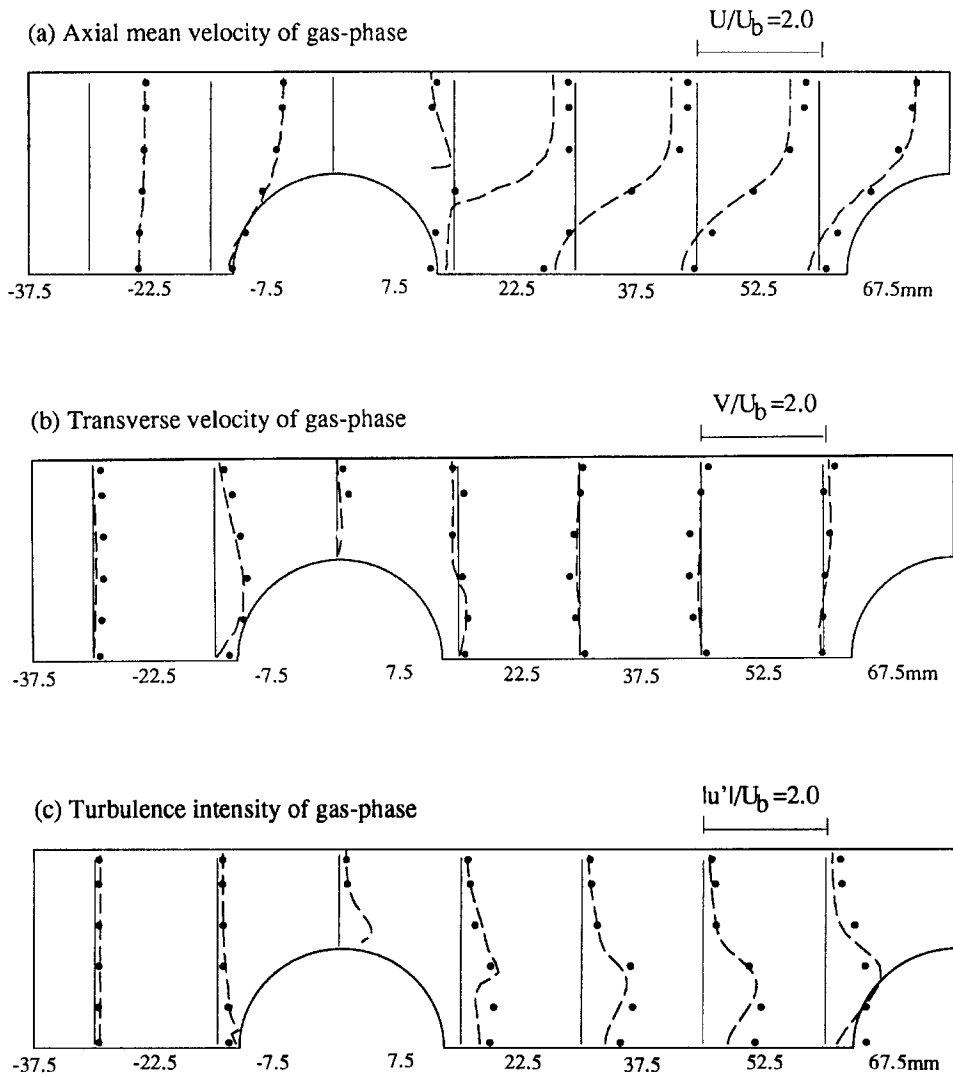Fig. 4. Computational domain and grids (196 × 32).

Fig. 5. Comparisons of mean velocity profiles and turbulence intensity of gas phase with experimental data: (----) prediction; (●) experimental data; (———) position of measurement and origin.

numerical prediction and to investigate the particulate behaviour in tube bank system. In this section, predictions using the present computational model are compared with measured data of the mean axial and transverse velocity profiles of both phases, the distribution of particle concentration and the turbulent intensity of the gas phase. Then the influence of different particle sizes on the velocity profile of the particulate phase in the tube bank is discussed on the basis of the experimental observation.

The flow conditions used in the computation for the comparison with the experiment are: the bulk velocity $U_b = 11.2$ m/s; the particle diameter size $d_p = 66\,\mu$m; the particle material density $\rho_s = 2{,}990$ kg/m^3; the gas density $\rho_g = 1.17$ kg/m^3; the particle volumetric fraction $\alpha = 3 \times 10^{-5}$; the mean normal and tangential restitution coefficients $e_p^{-N} = e_p^{-T} = 0.9$.

Figure 4 shows the computational domain and grids used for comparing the numerical prediction with the measurements carried out in the wind tunnel indicated in Figs 1 and 2. The measured data at the station $x = -37.5$ mm is taken as the inlet boundary conditions for the present computation. The flow is assumed to be fully developed at the outlet boundary and to be symmetrical at the top and bottom of the computational domain, which is slightly different from the experimental observation for the particulate phase due to the gravity acting in the direction perpendicular to the flow.

Figures 5 and 6 present comparisons of the predicted mean velocity profiles and turbulent intensity of the gas flow with measured data at the different sections in the tube bank. The agreement of the numerical prediction with the measurement is quite good for most of the sections, except there exists a slight (i.e. 8%) underprediction of mean axial velocity in the region just after the first tube. Some discrepancies between the predicted and measured gas
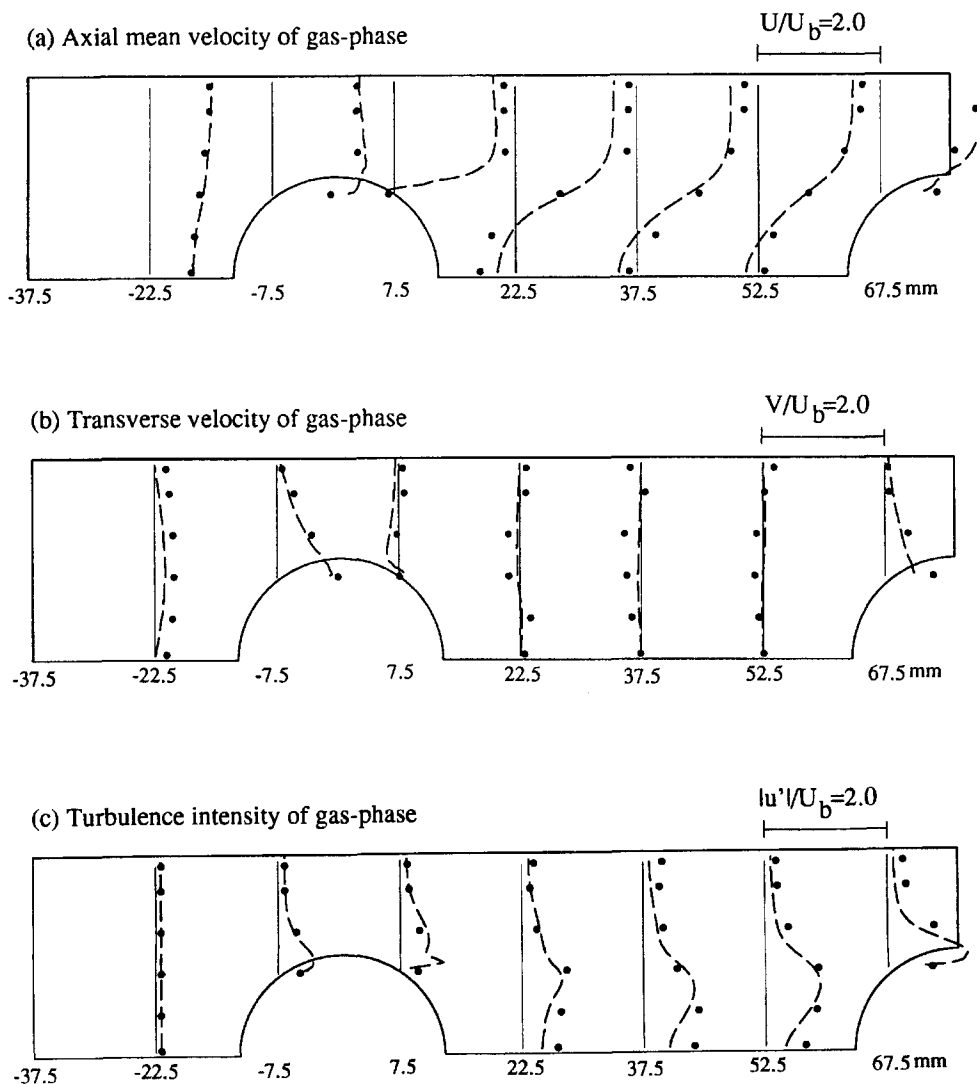

Fig. 6. Comparisons in other sections, for legend see Fig. 4.

(a) Axial mean velocity of particulate phase $U_p/U_b=2.0$

-37.5   -22.5   -7.5   7.5   22.5   37.5   52.5   67.5 mm

(b) Transverse mean velocity of particulate phase $V_p/U_b=2.0$

-37.5   -22.5   -7.5   7.5   22.5   37.5   52.5   67.5 mm

(c) Normalised particulate concentration $\rho_p/\rho_{ref}=2.0$

-37.5   -22.5   -7.5   7.5   22.5   37.5   52.5   67.5 mm
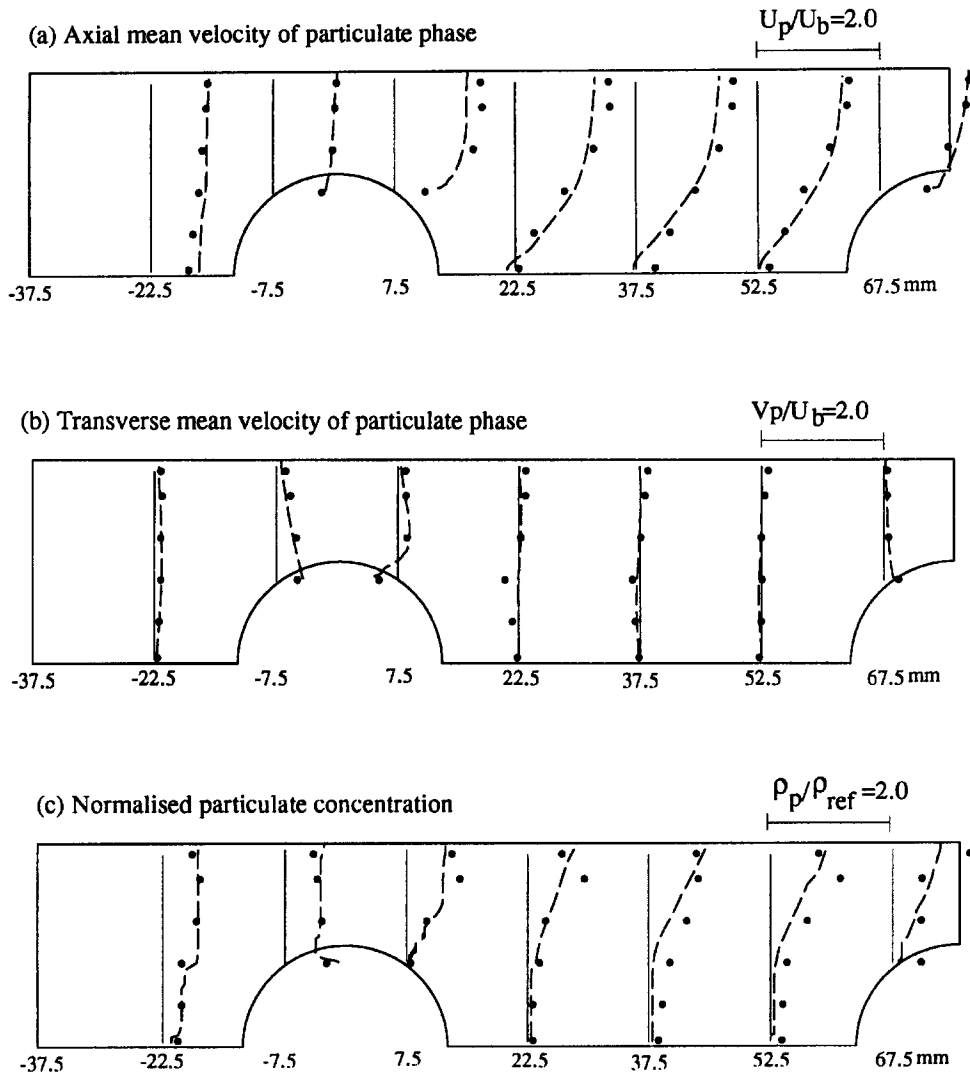
Fig. 7. Comparisons of mean particulate velocity profiles and particle concentration with experimental data: (----) prediction; (●) experimental data; (——) position of measurement and origin.

turbulence intensity are also observed in the region close to the second tube.

Comparisons of numerical predictions for the particulate phase with the measurements are shown in Fig. 7, where both mean particulate velocity profiles and concentration at the different sections are presented. It can be seen that the present Eulerian model yields a very good agreement between numerical predictions for the particulate phase with the measured data. The underprediction of the peak flow velocity after the first tube is, probably in part, due to the gas flow underprediction. The mean particle rebounding behaviour from the tube surface has been properly accounted for, as can be inferred by observing the comparison of the mean velocity profile at station, $x = -7.5$ mm.

The particulate concentration at a measurement position is obtained by recording the number of particles detected in a certain time and dividing by the total detecting time to obtain the number of particles detected per second. Then, it is divided by a maximum value to get the normalized measured particle concentration. The numerical results of the particle concentration are normalized by a maximum value in the computational domain. With the normalization procedure described above, the distribution of the particle concentration in the tube bank can be compared for the measurement and computations. Although the comparison of absolute values of particle concentration cannot be made, the global tendency of the normalized concentration distribution in the tube bank is found to be quite consistent for the experimental and computational data. Under the present flow condition (the Stokes number $S_t = 17$ based on the tube diameter or $S_t = 1$ based on the hydraulic diametric of the wind tunnel), the released particles have high inertia and mostly go straight through the gap between the tubes. The mean particulate flow is mainly

controlled by the particle–wall collision and is hardly affected by the gas flow. Hence, few particles can be found behind the first tube and downstream as far as the second tube.

To gain a better understanding of the flow behaviour of the particulate phase in the tube bank, the experimental results in terms of the mean and fluctuating velocities for both the gas and particulate phases with two different particle sizes ($d_p = 66$ and 93 μm) are presented in Figs 8 and 9.

Figure 8(a) shows the mean axial velocity profiles at seven axial locations. There is little difference of mean axial velocities between the gas and particulate phases before the flow impinges the first tube. It is interesting to see that the velocity of both the gas and smaller particles ($d_p = 66$ μm) has considerably increased at -7.5 mm due to the constriction of the first tube while the velocity of the larger particles ($d_p = 93$ μm) does not significantly increase until at the station of 7.5 mm because of their larger response time. The velocity profiles of the gas phase are higher than that of the particulate phase and the difference decreases as the flow diffusion behind the first tube because the larger particles have less diffusion.

A large recirculation zone for the gas flow can be identified easily in the wake of the first tube, but not for the particulate flow, in particular, for the larger particles. Thus, it is noted that the flow patterns of the particulate phase through the tubes are substantially different from those of the gas phase, particularly for larger particles.

The quite different behaviour of the particulate phase is found from the axial velocity fluctuation profiles as shown in Fig. 8(b). The fluctuating velocity profiles of the particulate phase for each of the two particle sizes are higher than that of the gas phase at all stations except in the wake of the first tube. The larger the particles, the higher is their velocity fluctuation. This behaviour of high fluctuation velocity for the particulate phase in gas–particle flows was also observed by other workers, such as Kliafas and Holt (1987) for a 90° bend flow and theoretical results obtained by Reeks (1993) and Simonin et al. (1994). The fluctuating velocity profiles in the front of the first tube reveal more difference between the gas and particulate phases than that behind the tube.

Figure 9 shows the mean and fluctuating transverse velocity profiles of both the gas and particulate phases. Also one can see the difference of flow patterns between the gas and particulate phases from the mean transverse velocity profiles [see Fig. 9(a)]. In the front of the first tube, the larger particles have smaller transverse velocity than the smaller particles and the gas phase. This reveals that the larger particles are less influenced by the gas flow and they are most likely to impinge straight on the tube surface. Such large particles also respond slowly to changes in the mean gas flow, so that their motion is considerably influenced
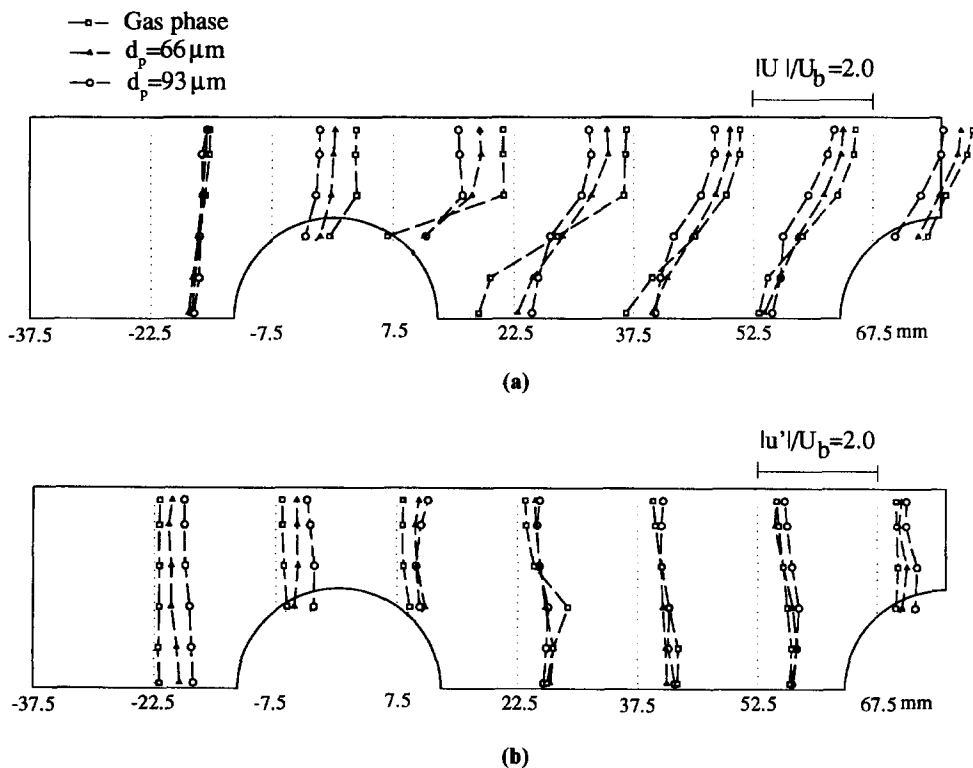

Fig. 8. Experimental results of axial mean and fluctuating velocity profiles in the in-line tube bank.
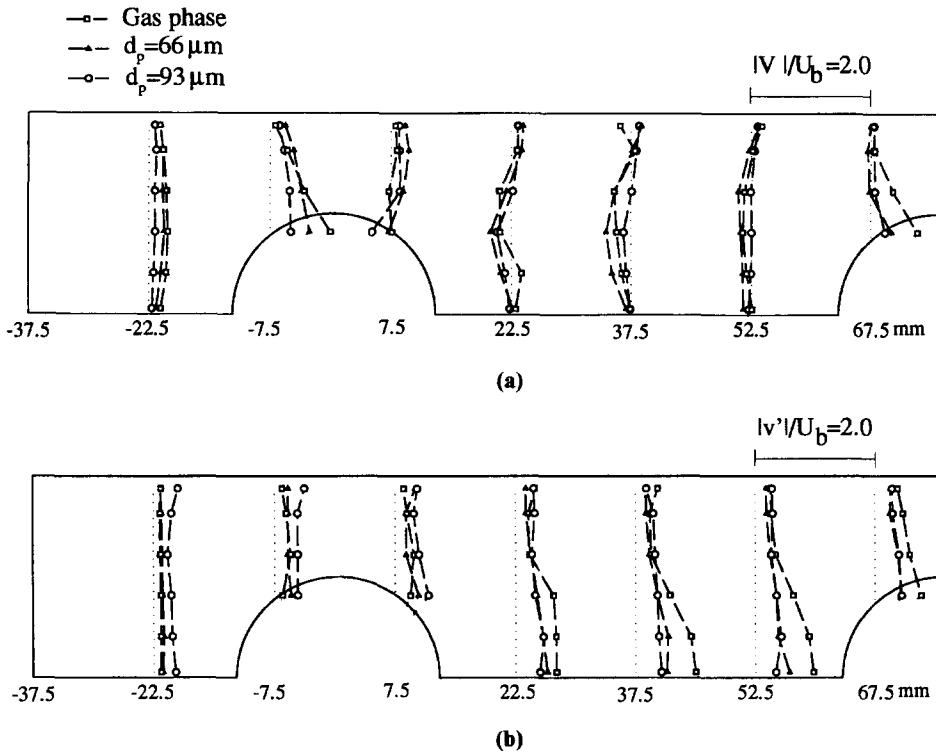
Fig. 9. Experimental results of transverse velocity profiles in the in-line tube bank.

by the particle–wall collision process in the cross flow through the tube banks.

The negative transverse velocity profiles for both the gas and particulate phases are found in the wake of the first tube. For the gas phase this is because a big recirculation zone is formed behind the tube while for the particulate phase this may be because of rebounding particles from the top tube.

A similar feature for the transverse fluctuation velocity to the axial component is found in the front of the first tube where the larger particles have large fluctuating velocities. However, smaller fluctuation profiles for the particulate phase than the gas phase are found in the wake of the first tube, probably because there is a large recirculation zone for the gas phase but not for the particulate phase between the two tubes.

5. CONCLUSION

Complementary numerical and experimental investigations have been described in this paper for turbulent particle-laden gas flows in an in-line tube bank. For the numerical calculations, an Eulerian model with generalised Eulerian boundary conditions and including a particle–wall collision model for the particulate phase is utilised. The RNG-based k–ε turbulence model is used to account for the turbulence effects of the gas phase while the particulate turbulence diffusivity is related to the turbulent viscosity

of the gas phase. The experimental investigation is carried out in an in-line tube bank located in a horizontal wind tunnel by the use of the laser Doppler anemometry (LDA) technique. The results of measurements of the mean velocities of two phases, gas turbulence intensity and particle concentration are used to validate the numerical predictions. Good agreement between the predictions and measurements is obtained. The comparison of experimental results of the different size particles with the gas phase reveal that the flow patterns of the particulate phase through the tubes are substantially different from those of the gas phase, particularly for larger particles, and that particle motion is considerably influenced by the particles colliding with the tube surface. The investigation of tube bundle erosion due to the effect of fluid motion on the particle motion and the study of the modification of the heat transfer performance in the presence of particle suspensions become very interesting research topics following the present work.

NOTATION

a, b, c, A, B	coefficients in particulate boundary equations
A_n	face area of control volume
C_N, C_T, C_m	particle–wall collision model coefficients
$C_\mu, C_{\mu 1}, C_{\mu 2}$	turbulence model constants
d_p	particle diameter
D	diameter of tube
D_p	particulate turbulent diffusivity
e_p^{-N}, e_p^{-T}	mean restitute coefficients
f	drag correction factor
F_G	gravity force
F_D	aerodynamic drag force
F_{WM}	particle–wall momentum transfer force
h	distance from the wall
Kn	Knudsen number, l_{gp}/L_D
k	turbulent kinetic energy
l_{gp}	gas–particle interaction length
L_D	hydraulic diameter
P	static pressure of gas phase
P_k	turbulence production
P_t	pitch in direction parallel to flow
q	averaging parameter
Re	Reynolds number
S_t	Stokes number
t_e	eddy characteristic time
t_p	particle relaxation time
u, v, W	mean velocity
u'	fluctuating velocity
U_b	bulk velocity
x	Cartesian coordinate
y^+	dimensionless distance from wall

Greek letters

α	inverse Prandtl number
ε	dissipation rate of turbulent kinetic energy
μ_{gt}	turbulent viscosity of gas phase
v_l	laminar kinematic viscosity of gas phase
$v_{g,\text{eff}}$	effective viscosity of gas phase
v_p	turbulent viscosity of particulate phase
ρ_g	bulk density of gas phase
ρ_p	bulk density of particulate phase
ρ_s	material density of particulate phase

Subscripts

g	gas phase
h	distance from wall
N	normal direction
p	particulate phase
T	tangential direction
w	wall
i, j	1, 2 (x, y)

Superscripts

i, j	1, 2 (x, y)
N	normal direction
T	tangential direction

REFERENCES

Adeniji-Fashola, A. and Chen, C. P. (1990) Modelling of confined turbulent fluid–particle flows using Eulerian and Lagrangian schemes. *Int. J. Heat Mass Transfer* 33, 691–701.

Bendat, J. S. and Piersol, A. G. (1971) Random data: analysis and measurement procedures. Wiley-Interscience, New York.

Celik, J., Patel, V. C. and Landweber, L. (1985) Calculation of the mean flow past circular cylinders by viscous-inviscid interaction. *J. Fluids Engng* 107, 218.

Chen, C. P. and Wood, P. E. (1985) A turbulence closure model for dilute gas–particle flows. *Can. J. Chem. Engng* 63, 349–360.

Cho, N-H. and Fletcher, C. A. J. (1991) Computation of turbulent conical diffuser flows using a non orthogonal grid system. *Comput. Fluids* 19, 347–361.

Cho, N-H., Fletcher, C. A. J. and Srinivas, K. (1991) Efficient computation of wing body flows. *Lecture Notes in Physics*, Vol. 371, pp. 167–191, Springer, Berlin.

Durst, F., Melling, A. and Whitelaw, J. H. (1981) *Principles and Practice of Laser-Doppler Anemometry.* Academic Press, London.

Faghri, M. and Rao, N. (1987) Numerical computation of flow and heat transfer in finned and unfinned tube banks. *Int. J. Heat Mass Transfer* 30, 363.

Fan, J., Zhou, D., Jin, J. and Cen, K. (1991) Numerical calculations of tube bundles erosion by turbulent particle-laden gas flows. *Chem. Engng Commun.* 104, 209–225.

Fletcher, C. A. J. (1991) *Computational Techniques for Fluid Dynamics*, Vol. 2: Specific Techniques for Different Flow Categories, 2nd edn. Springer, Heidelberg.

Fletcher, C. A. J. (1993) Gas particle industrial flow simulation using RANSTAD. In *Surveys in Fluid Mechanics*, ed. R. Narasimha, Vol. 18, Parts 3 & 4, pp. 657–681, Indian Academy of Science, Bangalore, India.

Fletcher, C. A. J. and Bain, J. G. (1991) An approximate factorisation explicit method for CFD. *Comput. Fluids* 19, 61–74.

Gore, R. A. and Crowe, C. T. (1989) Effect of particle size on modulating turbulent intensity. *Int. J. Multiphase Flow* 15, 279–285.

Halim, M. S. and Turner, J. T. (1986) Measurements of cross flow development in a staggered tube bundle. *Proceedings of the International Symposium on Applications of Laser Anemometry to Fluid Mechanics*, Lisbon, Portugal.

Ilias, S. and Douglas, P. L. (1989) Inertial impaction of aerosol particles on cylinders at intermediate and high Reynolds numbers. *Chem. Engng Sci.* 44, 81–99.

Kliafas, Y. and Holt, M. (1987) LDV measurements of turbulent air–solid two-phase flow in a 90° bend, *Exp. Fluids*, Vol. 15, 73–79.

Laitone, J. A. (1981) A numerical solution for gas-particle flows at high Reynolds numbers. *J. Appl. Mech.* 48, 465–471.

Launder, B. E. and Spalding, D. B. (1974) The numerical computation of turbulent flows. *Comput. Meth. Appl. Mech. Engng* 3, 269–289.

Melvlle, W. K. and Bray, K. N. C. (1979) A model of the two-phase turbulent jet. *Int. J. Heat Mass Transfer* 22, 647–656.

Menon, R. and Lai, W. T. (1991) Key considerations in the selection of seed particles for LDV measurements. *ASME Laser Anemometry* 2, 719–730.

Morsi, S. A. and Alexander, A. J. (1972) An investigation of particle trajectories in two-phase flow systems. *J. Fluid Mech.* **55**, 193.

Morsi, Y. S., Yang, W. and Atapattu, D. D. (1996) Experimental investigation of flow field in a tube bank in cross flow, *Proceedings of First Australian Conference on Laser Diagnostics in Fluid Mechanics and Combustion*, The University of Sydney, Australia, December, 1996, pp. 173–179.

Murray, D. B. and Fitzpatrick, J. A. (1992) The effect of solid particles on crossflow heat transfer in a tube array. *Exp. Therm. Fluid Sci.* **5**, 188–195.

Nowshiravani, S., Dybbs, A., Edwards, R. V. and Farrokhalaee, T. (1982) Velocity measurements in rod bundles. *Proceedings of the International Symposium on Applications of Laser Anemometry to Fluid Mechanics*, Lisbon, Portugal.

Orszag, S. A., Yakhot, V. and Flannery, W. S. et al. (1993) Renormalization group modeling and turbulence simulations. In *Near Wall Turbulent Flows*, eds. R. M. C. So, C. G. Speziale and B. E. Launder, pp. 1031–1046. Elsevier, Amsterdam.

Pourahmadi, F. and Humphrey, J. A. C. (1983) Modeling solid–fluid turbulent flows with application to predicting erosive wear. *Int. J. Phys. Chem. Hydro.* **4**, 191–219.

Reeks, M. W. (1993) On the constitutive relations for dispersed particles in nonuniform flows. 1: Dispersion in a simple shear flow. *Phys. Fluids* A **5**, 750–763.

Rhie, C. M. and Chow, W. L. (1983) Numerical study of the turbulent flow past an airfoil with trailing edge separation. *AIAA J.* **21**, 1525.

Rizk, M. A., Mostafa, A. A. and Abolfadl, M. A. (1993) Calculations of a particle-laden flate turbulent boundary layer. *ASME Gas–Solid Flows*-1993, FED-Vol. 166, pp. 169–176.

Sakakibara, J., Wicker, R. B. and Eaton, J. K. (1995) Measurements of the particle–fluid velocity correlation and the extra dissipation in a round jet. Technical Report IL-128, Thermosciences Division of Mechanical Engineering Department, Stanford University.

Schuh, M. J., Schuler, C. A. and Humphrey, J. A. C. (1989) Numerical calculation of particle-laden gas flows past tubes. *A.I.Ch.E. J.* **35**, 466–480.

Simoneau, R. J. and VanFossen, G. J. (1984) Effect of location in an array on heat-transfer to a short cylinder in crossflow. *Trans. ASME, J. Heat Transfer* **106**, 1453–1459.

Simonin, O., Deutsch, E. and Boivin, M. (1994) Large eddy simulation and second-moment closure model of particle fluctuating motion in two-phase turbulent shear flows. *Proceedings of Ninth Symposium on Turbulent Shear Flows*, eds F. Durst et al., Springer, Berlin, pp. 565–580.

Sommerfeld, M. (1992) Modelling of particle–wall collisions in confined gas–particle flows. *Int. J. Multiphase Flow* **18**, 905–926.

Soo, S. L. (1984) Development of theories on liquid solid flows. *J. Pipeline* **4**, 137–145.

Tu, J. Y. and Fletcher, C. A. J. (1994) An improved model for particulate turbulence modulation in confined two-phase flows. *Int. Commun. Heat Mass Transfer* **21**, 775–783.

Tu, J. Y. and Fletcher, C. A. J. (1995a) Numerical computation of turbulent gas–solid particle flow in a 90° bend. *A.I.Ch.E. J.* **41**, 2187–2197.

Tu, J. Y. and Fletcher, C. A. J. (1995b) Numerical analysis of turbulent gas–solid flows in in-line tube banks. In *ASME Gas–Solid Flows*-1995, FED-Vol. 228, pp. 309–318.

Tu, J. Y., Fletcher, C. A. J., Behnia, M., Reizes, J. A., Owen, D. and Johns, P. (1997) Prediction of flow and erosion in a coal fired power boiler and comparison with measurement. *ASME J. Engng Gas Turbines Power* **119**, 709–716.

Van Doormaal, J. P. and Raithby, G. D. (1984) Enchancements for the SIMPLE method for predicting incompressible fluid flow. *Numer. Heat Transfer* **7**, 147–163.

Vittal, B. V. R. and Tabakoff, W. (1987) Two-phase flow around a two-dimensional cylinder, *AIAA J.* **25**, 648–654.

Yakhot, V. and Orszag, S. A. (1986) Renormalization group analysisi of turbulence I. Basic theory. *J. Sci. Comput.* **1**, 3–51.